The randomly driven Ising ferromagnet: II. One and two dimensions

Johannes Hausmann† and Pál Ruján‡

† Fachbereich 8 Physik, Postfach 2503, Carl von Ossietzky Universität, D-26111 Oldenburg, Germany
‡ ICBM, Postfach 2503, Carl von Ossietzky Universität, D-26111 Oldenburg, Germany

Abstract. We consider the behaviour of an Ising ferromagnet obeying the Glauber dynamics under the influence of a fast-switching, random external field. In paper I, we introduced a general formalism for describing such systems and presented the mean-field theory. In this article we derive results for the one-dimensional case, which can be only partially solved. Monte Carlo simulations performed on a square lattice indicate that the main features of the mean-field theory survive the presence of strong fluctuations.

1. Introduction

This paper considers the randomly driven Ising model (RDIM) [1], introduced and discussed from a general point of view in paper I [2], in one and two dimensions. The main interest in studying such highly nonlinear nonequilibrium statistical physical systems lies in their possible applications for storage and other information processing tasks. Many biological systems, especially networks of real neurons, share common features with the RDIM in that they form strongly coupled systems driven by external stimuli acting in unison over a macroscopic number of elements in characteristic times shorter than the typical system relaxation time. Therefore, the Gaussian or Poissonian external 'noise' is transformed radically within the coupled system, leading to a 'correlated noise' with a lot of 'strange' properties. The mean-field theory was developed in paper I [2] for a random binary switching external field. Applications to cortical neurons will be discussed elsewhere.

The order parameter of the RDIM is a nonequilibrium stationary magnetization distribution, which undergoes a symmetry-breaking bifurcation at some critical field strength. The analytic structure of this distribution also changes in character as a function of the temperature and field parameters. Hence, transitions between a singular function with fractal support to a singular function with Euclidean support and further, to an absolutely continuous distribution can be observed. They can be seen in finite size effects and in the variance (the fluctuations) of the free energy. Similar transitions can be seen also in one dimension. However, the critical lower dimensionality of the RDIM remains one. Although the static critical exponent is a function of the field/temperature ratio, the dynamic exponent $z = 2$ remains unchanged. Some simple arguments will be given, supporting these results.

The situation is much more difficult in two dimensions, where only a Monte Carlo simulation approach was possible. The main difficulty is that computing the stationary properties of the system requires a large population of different trajectories. We found that it is

more convenient to use systems of moderate size than to rely on only a few dynamic trajectories. Even so, the simulations require a vast amount of computer resources. We solved this problem by using the Siemens–Nixdorf neurocomputer, SYNAPSE-1/N110, for quite a different task than what it was conceived for. This machine is basically a matrix-computer, allowing us to run many different systems in parallel. We were able only to determine roughly the phase diagram itself: we have no means at the moment for calculating the critical exponents.

The paper is organized as follows: in section 2 we consider the one-dimensional case. Although it cannot be fully solved, many interesting exact results can be derived. Section 3 deals with the Monte Carlo simulations we performed on finite square lattices. Many features of the mean-field dynamics are shown to survive the strong fluctuations characteristic to two-dimensional systems. However, in contrast to the mean-field approach, the two-dimensional model also displays an interesting spatial structure related to droplet dynamics. Comparisons between mean-field theory and two-dimensional results are systematically presented, including some preliminary results for hysteresis. Finally, we discuss our results in section 4.

2. RDIM in one dimension

2.1. The master equation

In his pioneering work, Glauber [3] defined a stochastic dynamics where only single spin flips are allowed and hence neither the magnetization (the order parameter), nor the energy is preserved (model A universality class, see [4]). Although introduced mainly for mathematical convenience, this dynamics is believed to describe appropriately many Ising-like systems.

The energy of an Ising chain with periodic boundary conditions is given by

$$E = -J \sum_{i=1}^{N} s_i s_{i+1} + \mu_B B(t) \sum_{i=1}^{N} s_i. \tag{1}$$

Following the notation of paper I [2] we denote by the vector $\vec{\mu} = (s_1, s_2, \ldots, s_i, \ldots, s_N)$ a given configuration of spins and by $\vec{\mu}_i = (s_1, s_2, \ldots, -s_i, \ldots, s_N)$ the same configuration but with the spin $s_i \to -s_i$ flipped. The external field is sampled from $\rho(B) = \frac{1}{2}\delta(B - B_0) + \frac{1}{2}\delta(B + B_0)$ at time intervals of length τ_B,

$$B(t) = B\rho(B) \sum_{n=0}^{\infty} \Theta(t - n\tau_B)\Theta((n+1)\tau_B - t). \tag{2}$$

As explained in paper I, the master equation has the form

$$\dot{P}(\{s_i\}; t) = -\hat{\mathcal{L}}_{B(t)} P(\{s_i\}; t)$$
$$= \sum_{i}^{N} w(\vec{\mu}|\vec{\mu}_i) P(\vec{\mu}_i; t) - P(\vec{\mu}; t) \sum_{i}^{N} w(\vec{\mu}_i|\vec{\mu}) \tag{3}$$

where $w(s_i) \equiv w(\vec{\mu}|\vec{\mu}_i)$ is the transition rate from a configuration $\{s_i\}$ into the state where only the ith spin is flipped, $\{-s_i\}$.

Strictly speaking, the system we are going to consider here will never reach the equilibrium Boltzmann distribution $e^{-\beta E}$, where $\beta = 1/k_B T$. Nevertheless, we require the detailed balance condition to be fulfilled for a constant value of the external field.

The transition probability $w(s_i)$ is determined by the constraint of detailed balance only up to a positive arbitrary function of the neighbouring spins, $f(s_{i-1}, s_{i+1})$. Since in one dimension

the phase transition is at $T_c = 0$, the choice of the transition probability influences the analytic form of the critical singularities [5]. In what follows we will use the form

$$w(s_i) = \frac{1}{2\alpha}\left[1 - s_i \tanh\left(K \sum_{j \in N(i)} s_j + H\right)\right] \tag{4}$$

where $K = \beta J$, $H = \beta \mu_B B$, α sets the time constant, and $N(i)$ denotes the set of nearest neighbours of spin i. Glauber introduced this form for $H = 0$ but used a slightly different one for $H \neq 0$. In one dimension one has then

$$w(s_i) = \frac{1}{2\alpha}[1 - s_i \tanh(K(s_{i-1} + s_{i+1}) + H)]. \tag{5}$$

For $H = 0$ the Liouville operator $\hat{\mathcal{L}}_B$ can be mapped onto a free-fermion spin-chain Hamiltonian [6]. This explains why the equations for the averaged spin products, $\langle \prod_{j \in \alpha} s_j \rangle$, decouple in subspaces which can be diagonalized by appropriate Fourier transformations. As shown below, this property is inherited by the first moments, $[\pi_\alpha(t)]$ of the stationary distribution $\mathcal{P}_s$.

2.2. Magnetization and correlation functions

Consider, for example, the time evolution of the local magnetization

$$m_i(t) = \langle s_i \rangle_t = \sum_{\{s_i\}} s_i P(\{s_i\}; t) \tag{6}$$

which can be obtained from (3) as

$$\dot{m}_i = -2\langle s_i w(s_i) \rangle_t = \frac{1}{\alpha}[-m_i(t) + \langle \tanh(K(s_{i-1} + s_{i+1}) + H) \rangle_t]. \tag{7}$$

In order to make the relationship to chaotic maps more evident, we use now the 'coarse grained' form [2] of (3). Formally, this procedure corresponds to a forward Euler discretization of (7), setting the time step equal to τ_B, and measuring time in units of $\alpha = \tau_B$:

$$m_i(t+1) = \langle \tanh(K(s_{i-1} + s_{i+1}) + H) \rangle_t$$
$$= a + \tilde{\gamma}\frac{m_{i-1}(t) + m_{i+1}(t)}{2} + b\langle s_{i-1} s_{i+1} \rangle_t \tag{8}$$

where $\gamma = \tanh 2K$, $h = \tanh H$, and

$$a = \frac{h}{2}\left(\frac{1 - \gamma^2}{1 - h^2\gamma^2} + 1\right) \tag{9}$$

$$\tilde{\gamma} = \gamma\left(\frac{1 - h^2}{1 - h^2\gamma^2}\right) \tag{10}$$

$$b = \frac{h}{2}\left(\frac{1 - \gamma^2}{1 - h^2\gamma^2} - 1\right). \tag{11}$$

Similarly, for the correlation function

$$c_{i,j} = \langle s_i s_j \rangle_t \tag{12}$$

one obtains

$$\dot{c}_{i,j} = -2\langle s_i s_j (w(s_i) + w(s_j)) \rangle_t \tag{13}$$

leading to the map

$$c_{i,j}(t+1) = \tfrac{1}{2}\langle s_j \tanh(K(s_{i-1} + s_{i+1}) + H) + s_i \tanh(K(s_{j-1} + s_{j+1}) + H) \rangle_t \tag{14}$$

where the time unit is now set to $\alpha = 2\tau_B$. These recursions can be written again in terms of the variables a, b and $\tilde{\gamma}$, equations (9)–(11).

For $H = 0$ one has $\tilde{\gamma} = \gamma$ and, as shown by Glauber [3], the slowest relaxation time equals the inverse of the smallest eigenvalue of the magnetization subspace, equation (7). This relaxation time diverges with the square of the static correlation length (the dynamic critical exponent is $z = 2$).

For the binary field distribution of (2), define $H_0 = \beta\mu_B B_0$ and $h_0 = \tanh H_0$. Evaluating equations (9)–(11) at $h = \pm h_0$ shows that the map of the local magnetization (8) has two branches:

$$m_i(t+1) = \begin{cases} a + \tilde{\gamma}\dfrac{m_{i-1}(t) + m_{i+1}(t)}{2} + bc_{i-1,i+1}(t) & \text{with probability } \frac{1}{2} \\[2mm] -a + \tilde{\gamma}\dfrac{m_{i-1}(t) + m_{i+1}(t)}{2} - bc_{i-1,i+1}(t) & \text{with probability } \frac{1}{2} \end{cases} \tag{15}$$

where it is implicitly assumed that the time needed to switch the field is negligible, $\tau_{\text{switch}} \ll \tau_B$.

From equation (15) it is evident that the map for the local magnetization couples to a two-spin correlation, which in turn couples to higher-order correlations etc. Hence, the full dynamic map lives in a 2^N-dimensional space, as stated in paper I [2].

Nevertheless, some partial results can be obtained for the stationary distribution. Define a 'thermal' and a 'dynamical' average, $\langle\ldots\rangle$ and $[\ldots]$ respectively. In the stationary state one has $[\langle A(t+1)\rangle] = [\langle A(t)\rangle]$ for any spin-function A. The average of the local magnetization obeys

$$[m_i] = \frac{[\tilde{\gamma}]}{2}([m_{i-1}] + [m_{i+1}]) \tag{16}$$

where (recall that $\gamma = \tanh 2K$)

$$[\tilde{\gamma}] = \gamma\frac{1 - h_0^2}{1 - h_0^2\gamma^2}. \tag{17}$$

For the (translation-invariant) magnetization $m = \frac{1}{N}\sum_i m_i$ and two-spin correlation function $c_j = \frac{1}{N}\sum_i c_{i,i+j}$ one obtains equations formally similar to the ones solved by Glauber [3]. From (16), $[m] = [\tilde{\gamma}][m]$, thus except for $[\tilde{\gamma}] = 1$, the stationary magnetization vanishes. The stationary two-spin correlation function obeys

$$[c_j] = \frac{[\tilde{\gamma}]}{2}([c_{j-1}] + [c_{j+1}]) \tag{18}$$

which leads to

$$[c_j] = \eta^{|j|} \qquad \text{with} \quad \eta = \frac{1 - \sqrt{1 - [\tilde{\gamma}]^2}}{[\tilde{\gamma}]}. \tag{19}$$

In general, when expressing the Frobenius–Perron operator in the basis formed by all moments of spin-products $[\pi_\alpha^q(t)]$, the subspace of the *first* moments ($q = 1$) is closed and can be diagonalized by a Fourier transform. The remaining part, however, is intractable. For example, the second moment of the magnetization reads

$$[m^2] = [a^2] + 2[ab][c_2] + [\tilde{\gamma}^2][m^2] + [b^2][c_2^2] \tag{20}$$

and couples both to the first and to the second moment of the translation-invariant correlation functions, $[c_2]$ and $[c_2^2]$, respectively.

2.3. The $T_c = 0$ phase transition

As expected, in the stationary state the odd moments of the magnetization vanish at $T > 0$. By expanding $\tilde{\gamma}$ and η at low temperature one obtains, after straightforward calculations, that close to $T_c = 0$ the correlation length is in leading order

$$
\xi = -\frac{1}{\ln \eta} \sim
\begin{cases}
\frac{1}{2} e^{2K - H_0} & \text{if } 2K > H_0 \\
\frac{1}{2} \frac{1}{H_0 - 2K} & \text{if } 2K < H_0.
\end{cases}
\tag{21}
$$

Hence, in one dimension the RDIM has a critical line with continuously changing singularities at $T_c = 0$ for $\kappa \equiv H_0/2K \in [0, 1]$. The slowest relaxation time corresponds to the magnetization (order parameter) decay and can be computed as

$$
\tau_{\text{sys}}^{-1} = 2(1 - [\tilde{\gamma}]) \sim
\begin{cases}
\xi^{-2} & \text{if } \kappa < 1 \\
2 & \text{if } \kappa > 1.
\end{cases}
\tag{22}
$$

Consider first the case of a strong field, $\kappa > 1$. The field will align all spins in one iteration step, as evident from equation (22). Hence, the spins are almost always parallel to the driving field. Since $[\tilde{\gamma}]$ vanishes, there is no spontaneously broken symmetry and $[m] = 0$ due to the symmetry of the field distribution, $\rho(B) = \rho(-B)$.

For fields smaller than the critical field $\kappa_c = 1$ one obtains a true symmetry-breaking ferromagnetic phase. Interestingly enough, while the divergence of the correlation length decreases continuously according to equation (21), the critical dynamic exponent remains $z = 2$ up to and including $\kappa \leqslant 1$. A physical argument explaining this result is presented below.

2.4. Kink dynamics at $T = 0$

Consider now the transition probability $w(s_i)$ at $T = 0$, equation (5), which is a function of the three spins s_i, s_{i-1}, and s_{i+1}. Let us call an interface between two oppositely oriented spin domains a *kink*. If $\kappa = H_0/2K = 0$ and $T = 0$ each kink performs a random walk, moving with equal probability to the left or to the right. When two kinks become nearest neighbours, they annihilate because in the next time step the single spin left between them will flip with probability one.

Due to this annihilation process the number of kinks decreases steadily and in the end only very few are left. Two kinks situated at the typical distance ξ (the correlation length) will meet via diffusive motion in the characteristic time $\tau \sim \xi^2$, which explains why the critical dynamic index is $z = 2$. The situation is similar if one is close to (but not at) $T_c = 0$.

How does this picture change if we switch on the random external field ($\kappa > 0$)? The domains parallel to the external field start growing—both ends of such a cluster will move outwards. Once the field changes sign, these domains shrink again and the clusters of oppositely aligned spins grow. During a longer period of time these effects compensate each other and the surviving kinks effectively perform a random walk. However, the annihilation rate of kink-pairs is highly increased. Assume, for example, that after $2T$ iteration steps the external field had the value $+H_0$ $(T + n)$-times. The probability for this to happen is given by the Bernoulli distribution, $B_n^{2T} = \binom{2T}{n}(\frac{1}{2})^n$. During this time, a down-oriented domain whose original length was L_0 shrinks on average by $2n(2p - 1)$, where both kinks associated with the ends of the domain have moved inward during each of the n time steps with probability $p > \frac{1}{2}$ and outward with probability $q = 1 - p$. Hence, if $2n(2p - 1) \sim L_0$, the domain will be eliminated. p is a function of $\kappa = \frac{H_0}{2K}$, e.g. $p(\kappa = 0.2) = 0.982$. Due to the depletion of small clusters, the number of kinks decreases much faster than in the absence of the external field.
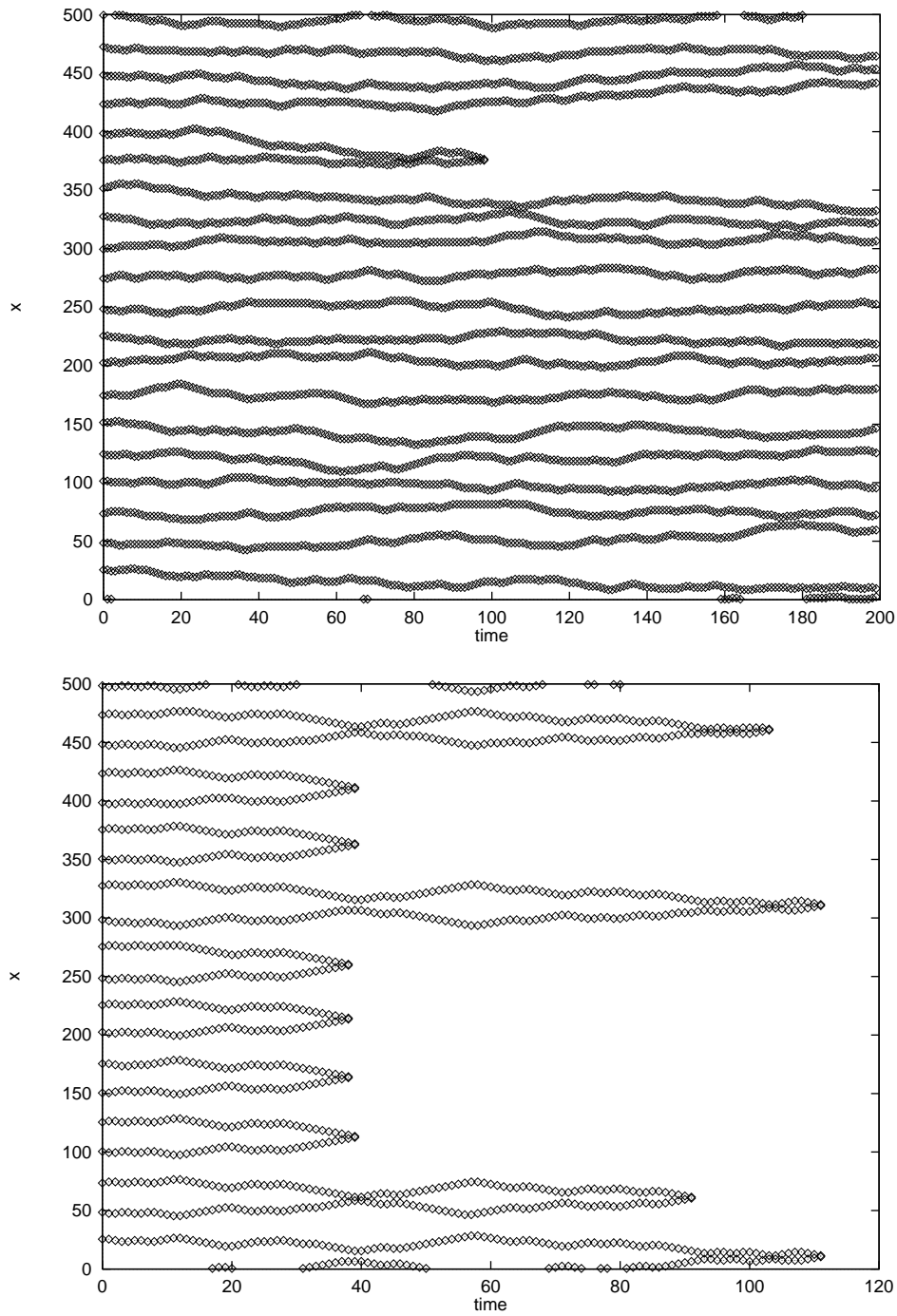
Figure 1. Diffusion of walls for $\kappa = 0$ (top) and $\kappa = 0.2$ (bottom), respectively. Note the different timescales.
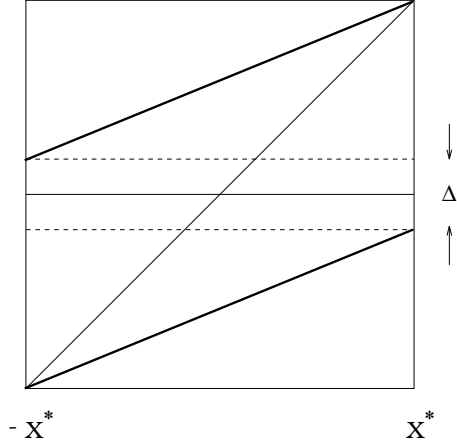
Figure 2. The truncated one-dimensional magnetization map for $\Delta > 0$.

This effect is illustrated by a numerical simulation in figure 1, showing the $T = 0$ dynamics of walls for $\kappa = 0$ and $\kappa = 0.2$, respectively.

Once only a few large clusters remain, however, their width becomes macroscopic. On this scale the kinks again perform a random walk and asymptotically one regains $z = 2$.

At finite temperatures, however, the presence of the field term facilitates the nucleation of new clusters, so that the correlation length (21) (the mean cluster size) is less divergent when $H_0 > 0$.

2.5. The magnetization distribution

Consider again the map (15). In the translational invariant sector one has

$$m(t+1) = \begin{cases} a + \tilde{\gamma}m(t) + bc_2(t) & \text{with probability } \frac{1}{2} \\ -a + \tilde{\gamma}m(t) - bc_2(t) & \text{with probablilty } \frac{1}{2}. \end{cases} \tag{23}$$

As already discussed, the magnetization couples to the correlation function $c_2(t)$, etc. A simple approximation to decouple the magnetization sector is using for $c_2(t)$ the stationary value $c_2 = \eta^2$. The resulting map corresponds to a Bernoulli-shift [7] and is shown graphically in figure 2. If the gap between the two branches is positive

$$\Delta = \frac{2(a + bc_2)(1 - 2\tilde{\gamma})}{1 - \tilde{\gamma}} > 0 \tag{24}$$

the corresponding stationary magnetization distribution is a Cantor set.

Since $a, b, (1 - \tilde{\gamma})$ are positive and $c_2 > 0$ for ferromagnetic interactions, the demarcation line between a fractal and a non-fractal magnetization distribution is given by

$$\tilde{\gamma} = \frac{1}{2} \tag{25}$$

independently of the actual value $c_2(t)$ might have. The time dependence of $c_2(t)$ induces nonlinearities in the map. Therefore, although the distribution remains fractal for $\tilde{\gamma} < \frac{1}{2}$, in general it is not a homogeneous Cantor set.

3. Monte Carlo simulations in two dimensions

We simulated the RDIM on a two-dimensional square lattice on the neurocomputer, SYNAPSE-1/N110. In the following sections we first describe a Monte Carlo Algorithm (MCA) designed

to make use of the computational power of SYNAPSE-1 and then present our numerical results. They include a phase diagram in the H-K-plane, magnetization distributions in the paramagnetic and ferromagnetic regimes, and a series of snapshots documenting the behaviour of the system.

3.1. The algorithm

SYNAPSE-1 is a workstation-driven coprocessor consisting of a systolic array of eight MA16 Neural Signal Processors. It was kindly put at our disposal by the ZFE of Siemens AG. Its hardware was designed to tackle typical problems encountered when simulating neural networks, namely calculations involving very large matrices. In order to efficiently make use of the C++-library interface supplied with SYNAPSE-1 for the RDIM, we devised a MCA that simulates multiples of eight lattices in parallel.

Consider a square lattice of spins $s_{ij}^k \in \{-1, 1\}$ of linear dimension L, where k numbers the system and $i, j = 1 \ldots L$ denotes the lattice position. Each of eight lattices is represented as a column vector s_ν by renumbering indices $\nu = iL + j$. The eight systems can thus be treated as *one* $8 \times L^2$-matrix. By setting $\nu \mapsto \nu + L^2$ for $\nu \leqslant 0$ and $\nu \mapsto \nu - L^2$ for $\nu > L^2$ we enforce helical boundary conditions. The neighbours of spin ν are $\mu = \nu \pm 1$, $\mu = \nu \pm L$.

In order to avoid metastable states induced by a simultaneous update of neighbouring spins we split the lattices into black and white sites in a checkerboard fashion, leading to *two* matrices encoding the eight systems. Note that when a lattice is divided up in this fashion, if L is odd, the sites in the first and last row have neighbours of their own colour. If L is even, the same is true for the first and last column of the lattice. For technical reasons we chose L to be odd.

To further simplify the updating scheme, a copy of the first and last L components of each lattice are included at the end (respectively, beginning) of each column vector. A Monte Carlo step now consists of a parallel update of all black sites followed by an update of all white sites (or vice versa).

From the well known Glauber dynamic rule equation (4), a spin is flipped under the following condition. Given a random number $z \in [0, 1]$ drawn from a uniform distribution, spin s_ν is updated according to

$$s_\nu \mapsto \begin{cases} -s_\nu & \text{if } z < \frac{1}{2}(1 - \tanh(s_\nu(K\Sigma_\mu s_\mu + H))) \\ s_\nu & \text{if } z \geqslant \frac{1}{2}(1 - \tanh(s_\nu(K\Sigma_\mu s_\mu + H))). \end{cases} \tag{26}$$

Usually, spins are either treated sequentially or chosen randomly. SYNAPSE-1 permits the parallel generation of (pseudo-) random numbers in a single Elementary Operation (ELOP) which can be piped through a function lookup table at no extra computational cost. For this reason we transform the flip condition equation (26) into

$$s_\nu \mapsto \begin{cases} -s_\nu & \text{if } \Sigma_\mu s_\nu s_\mu < \frac{1}{2K} \log(\frac{\frac{1}{2}-z'}{\frac{1}{2}+z'}) - s_\nu \frac{H}{K} \\ s_\nu & \text{if } \Sigma_\mu s_\nu s_\mu \geqslant \frac{1}{2K} \log(\frac{\frac{1}{2}-z'}{\frac{1}{2}+z'}) - s_\nu \frac{H}{K} \end{cases} \tag{27}$$

where z' is drawn from a uniform distribution in $[-\frac{1}{2}, \frac{1}{2}]$. The RHS of the flip condition is evaluated in two ELOPs: One to generate a matrix of random numbers piped through the function $z' \mapsto \frac{1}{2K} \log(\frac{\frac{1}{2}-z'}{\frac{1}{2}+z'})$ and one weighted matrix subtraction. The LHS also takes two ELOPs to calculate from the 'black' and 'white' matrices. Two further ELOPs are required to construct and evaluate a flip indicator matrix. Some more operations are necessary to fix boundary conditions and to evaluate the mean lattice magnetizations. This procedure is
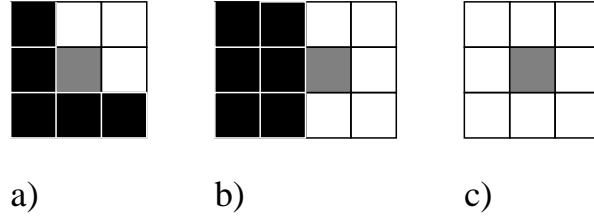
Figure 3. The basic spin-flip configurations, H_0 points upwards, up (down) spins are black (white), a spin turning up is drawn in grey. (*a*) a 'droplet'-flip, (*b*) a 'domain'-flip, (*c*) nucleation-flip.
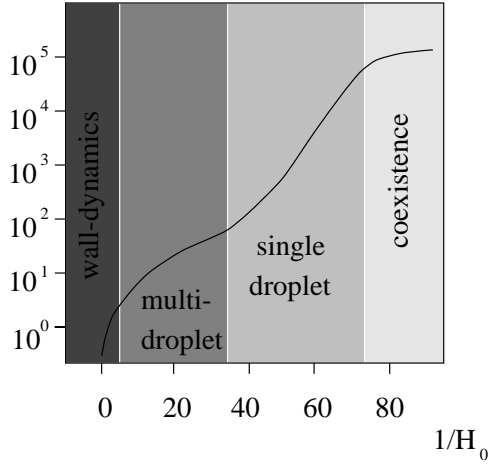

Figure 4. The average time spent in the metastable thermodynamic state as a function of inverse field-strength. The different domains are denoted according to their main relaxation mechanism.

applied sequentially first to the matrix holding the 'black' spins and then to the 'white' one to accomplish a complete Monte Carlo step.

Initially, the spins in a lattice are set to +1 with probability p and −1 with probability $1 - p$, where different values of p can be used for each lattice in one simulation run. The results for systems of linear dimension $L = 415$ are initialized with $p = 0, 0.2, 0.4, 0.5, 0.6, 0.8,$ and 1, in addition, there is one lattice in which the top half of all spins is set to +1 and the bottom half to −1. The external driving field is the same for each system. Simulations at smaller L consist of 64 systems initialized with $p = \frac{1}{2}$, but each with its own driving field trajectory.

Temperature K is measured in units of the critical temperature, $K \rightarrow \frac{K}{K_c}$, where $K_c = \frac{J}{k_B T_c} = \frac{1}{2} \ln(\sqrt{2} + 1) \approx 0.440\,69$ of the standard two-dimensional Ising model, i.e. $K = 1$ corresponds to the critical temperature for $H_0 = 0$.

3.2. Dynamics and phase diagram

In order to understand the dynamics of the two-dimensional RDIM in more detail, it is useful to consider first what happens to a cluster of parallel spins at $T = 0$, in analogy to kink dynamics for the one-dimensional case. Transition rates at $T = 0$ are either 0, 1, or $\frac{1}{2}$. Recalling that K is measured in units of K_c, define $\kappa' := \frac{H_0}{2K} = \kappa K_c$. Consider now a square cluster of $2N \times 2N$ parallel spins under the influence of an anti-parallel external field. First, if $0 < \kappa' < 1$, the
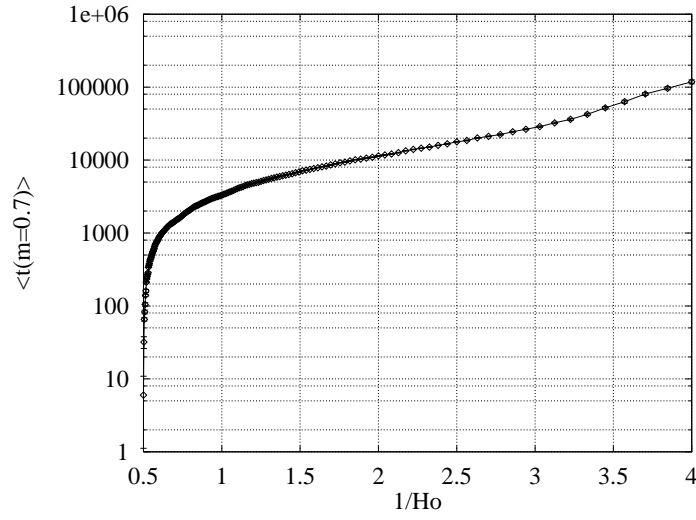
Figure 5. The average first-passage time from $m = -1$ to $m = 0.7$ at $K = 1.25$ as a function of inverse field-strength. $\langle t(m = 0.7) \rangle$ is calculated from an ensemble of 64 systems with linear dimension $L = 143$.
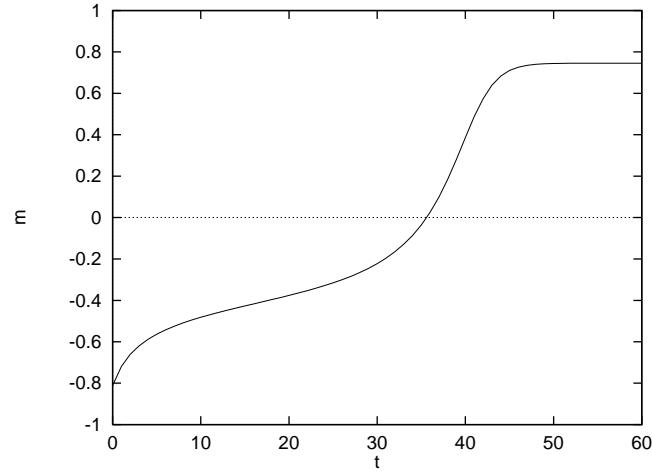

Figure 6. Mean-field iteration m versus time t in an unfavourable field for $\frac{H_0}{K} = 0.057$ and $K = 1.2$, which is slightly above the critical field.

spins at the corners of the cluster flip with probability $p = 1$, all other remain anti-parallel to the field (as shown in figure 3(*a*)). Thus the cluster disappears if the external field remains constant for $2N - 1$ consecutive steps. Secondly, if $1 < \kappa' < 2$, such a cluster will be destroyed in N steps, due to the fact that all but inner spins will flip with $p = 1$. Thirdly, at $\kappa' > 2$ we arrive at a driven paramagnetic phase. Regardless of their position, all spins will flip into the direction of the driving field with $p = 1$. For the case of $\kappa' = 0$, $\kappa' = 1$, or $\kappa' = 2$, corner, edge, and inner spins flip with $p = \frac{1}{2}$. This implies that, e.g. for a strong driving field with $\kappa' = 2K_c$, nucleation flips (see figure 3(*c*)) may take place *inside* the cluster, creating magnetic swiss cheese.
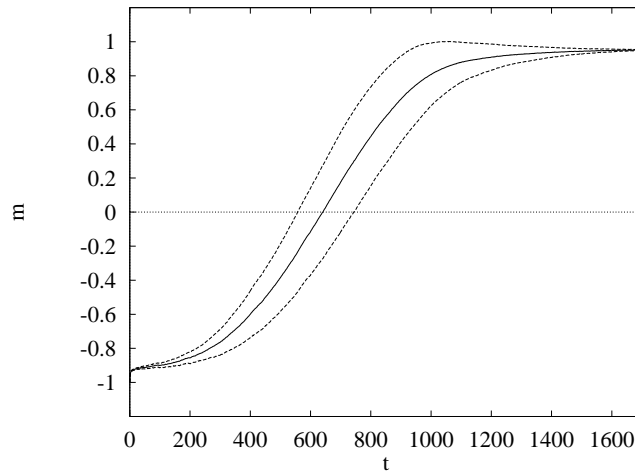
Figure 7. Monte Carlo simulation in an unfavourable field for $\frac{H_0}{K} = 0.08$, $K = 1.2$, $\tau_B = 1$, and linear dimension $L = 143$. The full curve shows the average magnetization in an ensemble of 64 systems, m, as a function of time t. The broken curves mark a 1-σ range around the mean. All systems start with all spins down, i.e. $\forall v : s_v = -1$.
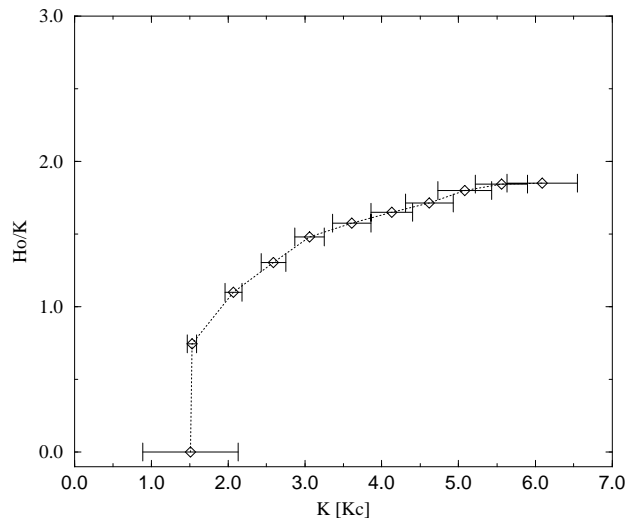

Figure 8. Phase diagram of the two-dimensional RDIM from Monte Carlo simulation of 64 systems of linear dimension $L = 63$.

The transition probabilities of the processes shown in figure 3 increase with increasing field strength. At small fields the (*a*)-type flip is prevalent, resulting in a radial growth (shrinkage) of clusters. Although energetically more expensive, the (*b*)-type flip has a large entropy contribution and results in long-wavelength growth of flat domain walls. The nucleation process shown in flip (*c*) has the smallest probability.

What happens when switching the field instantly from the equilibrium state at $-H_0$ into the unfavourable direction H_0? The system relaxes from the now metastable state to the new equilibrium value. Obviously, the lifetime of the metastable state depends on the strength
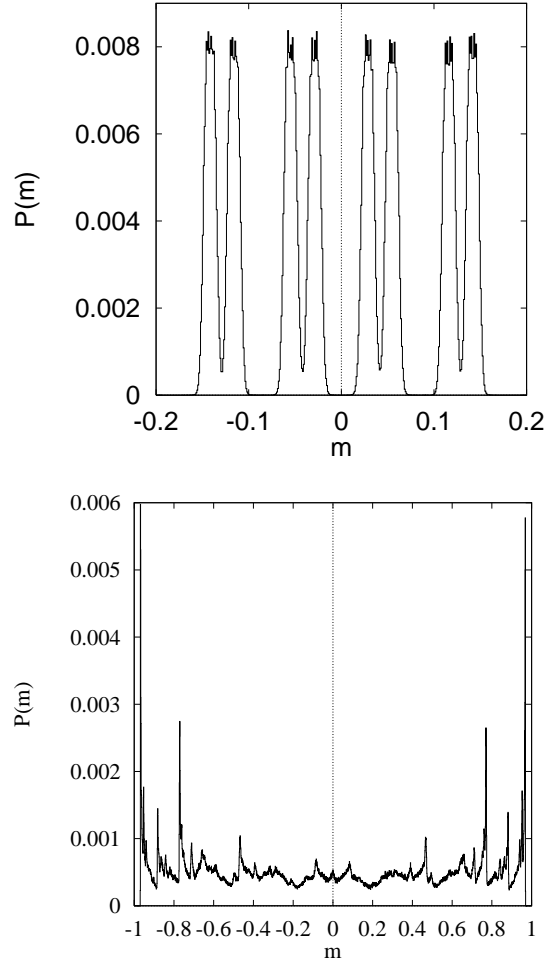
Figure 9. Top: magnetization distribution for the square lattice RDIM averaged from eight different initial conditions for $K = 0.4$, $\frac{H}{K} = 0.5$, $\tau_B = 1$, and linear dimension $L = 415$. Here, the simulation covers more than 2×10^5 Monte Carlo sweeps. Note the similarity to figure 1 of paper I. Bottom: $K = 1$, $\frac{H}{K} = 1$, $\tau_B = 1$, and $L = 415$. The simulation run covers close to 2×10^5 Monte Carlo sweeps. Compare this to figure 2 of paper I.

of the applied field. This scenario has been discussed in detail in the ferromagnetic phase using droplet theory and Monte Carlo simulations (see, for example, [8]). Here, four distinct field intervals, shown schematically in figure 4, were identified in which the lifetimes markedly differ due to different decay mechanisms. A numerical result for $K = 1.25$ is shown in figure 5, where we approximated the metastable lifetimes by measuring the average first passage times (FPT) from $m = -1$ to $m = 0.7$ in Monte Carlo steps. Figures 6 and 7 show examples of the time development of the magnetization from the metastable state to the new equilibrium for the mean-field and two-dimensional model.

We calculated numerically a phase diagram in the $K - \frac{H}{K}$-plane for the two-dimensional RDIM, figure 8. Similar to the mean-field and one-dimensional model, there is a paramagnetic, a ferromagnetic (and a driven paramagnetic) phase. Note that for $K \mapsto \infty$, the phase boundary should remain below $\kappa' = 2$. We are currently in no position to assess this. Also, the behaviour
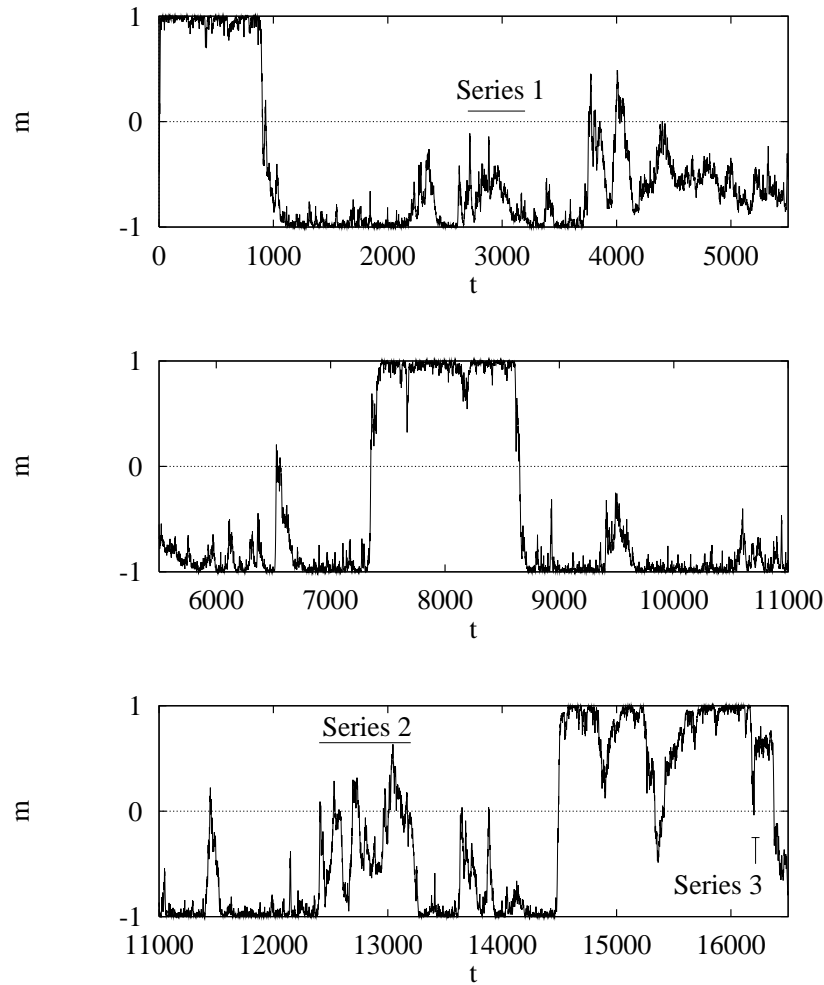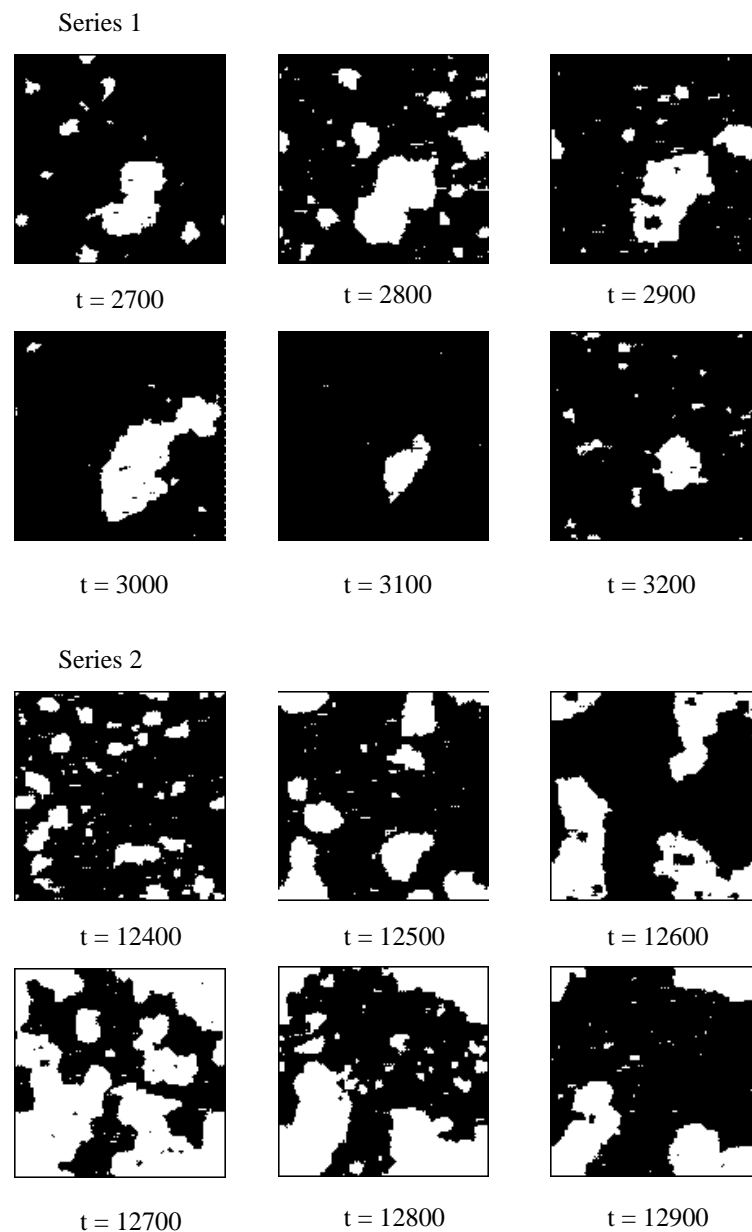
Figure 10. Time series of the mean magnetization of the RDIM. Parameters are $K = 2$, $\frac{H}{K} = 1$, $\tau_B = 1$, and the linear dimension is 128. Note that here the boundary conditions are periodic. Snapshots of the system are shown in series 1, 2, and 3 on the next pages.

around $K = 1$ does not seem to correspond to the first-order dynamic freezing transition seen in the mean-field theory, rather a second-order transition is likely. Very recently, Acharyya [9] studied a Monte Carlo simulation of the two-dimensional RDIM for a driving field uniformly distributed in $[-H_0, +H_0]$ using Metropolis dynamics. His results for the paramagnetic–ferromagnetic phase transition agree qualitatively with ours.

3.3. The paramagnetic phase

If the external field is above its critical value, $H_0 > H_c$, the stationary phase of the RDIM is paramagnetic. In this phase the system relaxes relatively fast to the equilibrium state, except close to H_c, where critical slowing down sets in due to the type-I intermittency effects discussed in the previous section.

This behaviour of the average magnetization is shown in figure 7 and is probably enhanced

Series 1

t = 2700   t = 2800   t = 2900

t = 3000   t = 3100   t = 3200

Series 2

t = 12400   t = 12500   t = 12600

t = 12700   t = 12800   t = 12900

Figure 10. (continued)

by local correlations not taken into account in the mean-field approximation. If the random field is switched on, close but above H_c the critical slowing down is dramatically enhanced. Further away from the phase transition point the dynamics is—similarly to the one-dimensional case—determined by the nucleation and radial growth (shrinking) of droplet-like clusters.

As expected from the mean-field results, the RDIM can display a fractal magnetization distribution at higher fields. This is shown in figure 9. Thermal fluctuations and finite size effects wash out the fine structure of the multifractal magnetization distribution predicted by
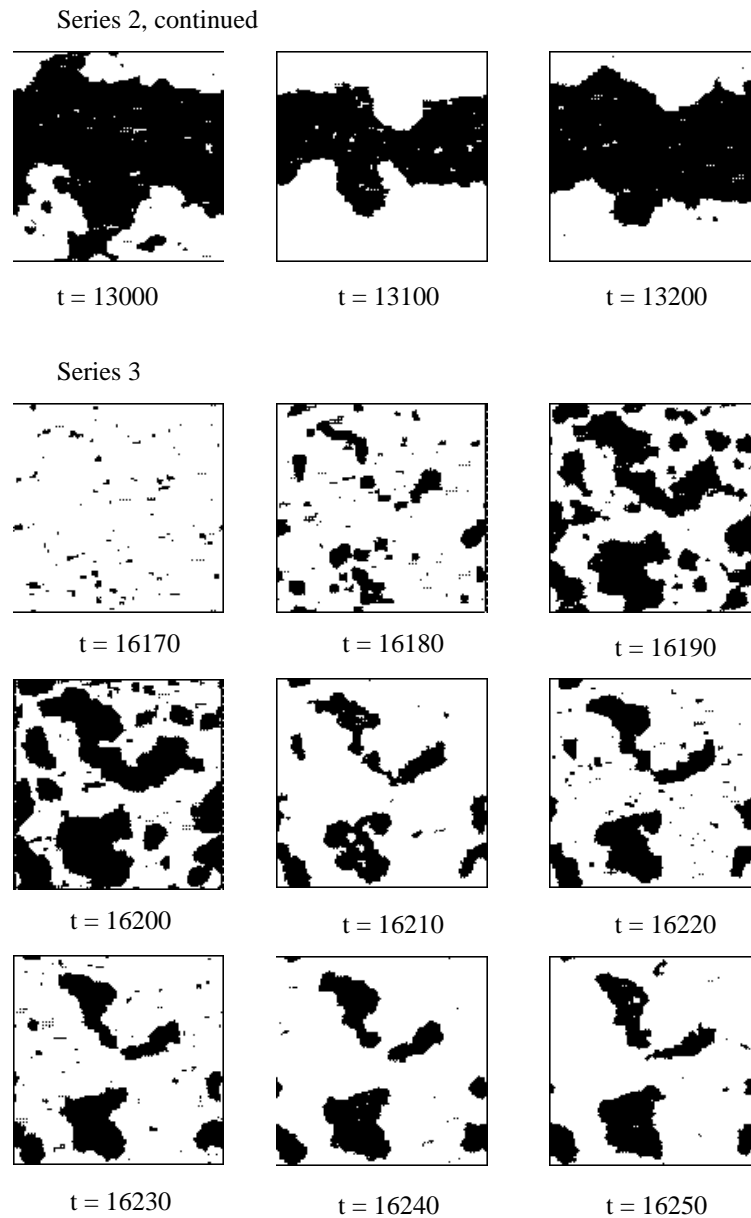
Series 2, continued

t = 13000   t = 13100   t = 13200

Series 3

t = 16170   t = 16180   t = 16190

t = 16200   t = 16210   t = 16220

t = 16230   t = 16240   t = 16250

Figure 10. (continued)

the mean-field calculations. However, the presence of sharp peaks in the distribution (and their scaling behaviour) demonstrates that some of the main features of the magnetization distribution survive the thermal fluctuations.

These peaks are related to long-lived droplets whose radius is large enough to allow them to stay alive even when a long series of unfavourable external field draws makes them shrink. It is, however, the competition between the two thermodynamically stable states which leads to a chaotic dynamics and strange attractors.
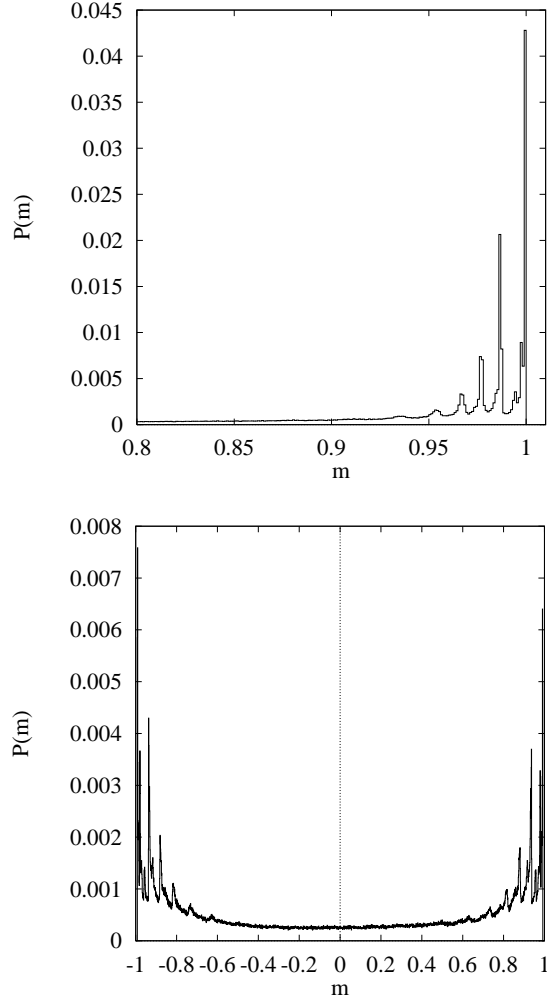
Figure 11. Top: magnetization distribution for the square lattice RDIM averaged from eight different initial conditions for $K = 2$, $\frac{H}{K} = 1$, $\tau_B = 1$, and linear dimension $L = 415$. We simulated more than 2×10^5 sweeps. Only the region from $m = 0.8$ to $m = 1.0$ is shown, the distribution is symmetric in m. It is similar to the mean-field distribution around the critical driving field H_c (cf figures 3 and 4 of paper I). Bottom: $K = 1.33$, $\frac{H}{K} = 0.75$, $\tau_B = 1$, and $L = 415$. We tracked 1.5×10^5 Monte Carlo sweeps. Here, the distribution resembles the mean-field distribution close to the critical driving field H_c.

3.4. The ferromagnetic phase

The situation is even more complex below H_c. The schematic dependence of the average time spent in a thermodynamically unstable state versus the inverse of the field strength is shown after [8] in figure 4.

The external-field sampling time τ_B should be chosen in either the strong or multidroplet regime (certainly not in the coexistence regime). By varying τ_B it seems possible to explore these different dynamic mechanisms in more detail. Figure 10 shows a simulation in the ferromagnetic phase where one can observe both a multidroplet (series 1 and 3) and a domain-
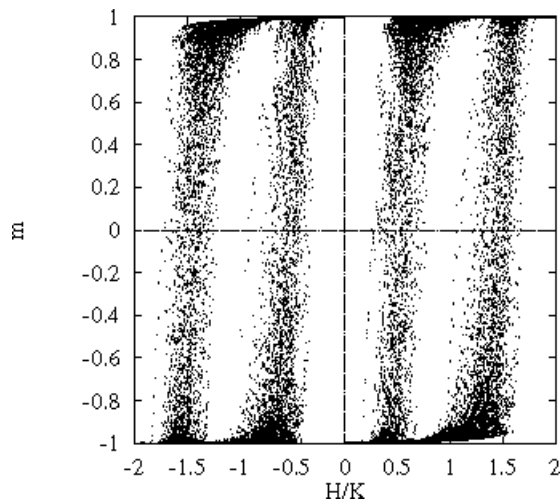
Figure 12. Hysteresis in the square lattice RDIM, showing the mean magnetization $m(t)$ versus the driving field $H(t)$, see equation (32) of paper I. Parameters are $\frac{A}{K} = \frac{H_0}{K} = 1$, $K = 2$, $\Omega = \frac{2\pi}{1000}$, and linear dimension $L = 415$. The simulation ran for more than 10^5 sweeps. See figure 8 of paper I for comparison.

wall type (series 2) dynamics. Again, the *spontaneous magnetization distribution* shows well-separated peaks, which can be seen in figure 11.

For the sake of completeness, we show in figure 12 a Monte Carlo simulation of the hysteresis measurement described in figure 8 of paper I [2]. Only the evolution of one system initialized with spins up/down with equal probability is displayed. Again, one can see that the thermal fluctuations are smoothing only the fine scale structure of the mean-field predictions—but the main features remain intact.

The results presented here leave open many questions regarding the 2D RDIM—an in-depth study by Monte Carlo simulation currently lies beyond our means. The theory and evolution of droplets and domains in the RDIM as well as hysteretic effects remain interesting research topics.

4. Summary and discussion

In this and our previous paper we have discussed in detail the properties of a simple Ising model subject to a fast-switching external field. In many ways, the situation is just the opposite as in quenched random systems. While there the defects, and hence the (local) fields are frozen relative to the spin degrees of freedom, which are (in principle) free to relax, in the RDIM the external field is the fast variable compared to the interacting spin system. From a 'technological' theoretical point of view the situation is, however, much easier. We expect that similar analytic results can be obtained for other random distributions as well. Strongly driven systems show rather peculiar properties, which one could use for increasing the storage properties of ferromagnetic materials. For example, it seems possible to use arithmetic coding in 'preparing' a semi-macroscopic ferromagnetic region to fall into a given distribution peak, as the ones shown in figure 9. An appropriately sensitive reading head could then discriminate between the different magnetization values. Such 'devices' could be tested first with the help of

Monte Carlo simulations. However, the main application domain for randomly driven systems might well be in biology. Further work in that direction is under progress.

Acknowledgments

References

[1] Ruján P and Hausmann J 1997 Stationary properties of a randomly driven Ising ferromagnet *Phys. Rev. Lett.* **79** 3339
[2] Ruján P and Hausmann J 1999 The randomly driven Ising ferromagnet: I. General formalism and mean-field theory *J. Phys. A: Math. Gen.* **32** 61
[3] Glauber R J 1963 Time-dependent statistics of the Ising model *J. Math. Phys.* **4** 294
[4] Halperin B I and Hohenberg P C 1977 Theory of dynamic critical phenomena *Rev. Mod. Phys.* **45** 435
[5] Pandit R, Forgács G and Ruján P 1981 Finite-size calculations for the kinetic Ising model *Phys. Rev.* B **24** 1576
[6] Felderhof B U 1970 *Rep. Math. Phys.* **1** 1
     Siggia E D 1977 Pseudospin formulation of kinetic Ising models *Phys. Rev.* B **16** 2319
[7] Grossmann S and Horner H 1985 Long time tail correlations in discrete chaotic dynamics *Z. Phys.* B **60** 79
[8] Rikvold P A, Tomita H, Miyashita S and Sides S W 1994 Metastable lifetimes in a kinetic Ising model: dependence on field and system size *Phys. Rev.* E **49** 5080
[9] Acharyya M 1998 Nonequilibrium phase transition in the kinetic Ising model: Dynamical symmetry breaking by randomly varying magnetic field *Phys. Rev.* E **58** 174